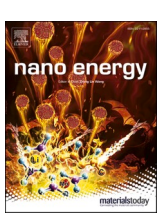
ELSEVIER

Contents lists available at ScienceDirect

Nano Energy

journal homepage: http://www.elsevier.com/locate/nanoen





Strongly-ligated perovskite quantum dots with precisely controlled dimensions and architectures for white light-emitting diodes

Shuang Pan ^{a,b,1}, Yihuang Chen ^{a,1}, Zewei Wang ^a, Yeu-Wei Harn ^a, Jiwoo Yu ^a, Aurelia Wang ^a, Marcus J. Smith ^{a,c}, Zili Li ^a, Vladimir V. Tsukruk ^a, Juan Peng ^{b,**}, Zhiqun Lin ^{a,*}

- ^a School of Materials Science and Engineering, Georgia Institute of Technology, Atlanta, GA, 30332, USA
- b State Key Laboratory of Molecular Engineering of Polymers, Department of Macromolecular Science, Fudan University, Shanghai, 200438, China
- ^c Air Force Research Labs-Aerospace Systems Directorate, WPAFB, OH, 45433, USA

ARTICLE INFO

Reywords: Strongly-ligated perovskite quantum dots Controlled dimensions and architectures Meniscus-assisted self-assembly CsPbBr₃ White LEDs

ABSTRACT

Despite impressive advances in the synthesis of perovskite quantum dots (PQDs), the ability to craft PQDs of the same dimension yet different architectures (e.g., solid vs. hollow) remains a grand challenge. Moreover, precise control over the architectures and assemblies of PQDs renders new optical and optoelectronic properties. Herein, we report on a robust amphiphilic star-like block copolymer nanoreactor strategy to rapidly create monodisperse solid and hollow PQDs of the same external diameter in-situ. The dimension of PQDs can be readily regulated by utilizing star-like copolymers. Compared to solid PQDs, as the inner diameter of hollow PQDs increases, their photoluminescence progressively blue-shifts. Moreover, stripe patterns of PQDs can be conveniently formed via meniscus-assisted self-assembly (MASA) and subsequently anion-exchanged to yield multi-colored stripes with a heterostructured transition zone. Conceptually, an array of PQDs including all inorganic lead-free and organic-inorganic PQDs, can be easily accessed for applications in lasers, LEDs, and solar cells.

1. Introduction

Colloidal perovskite nanocrystals with a generic chemical formula ABX_3 (e.g., $A^+ = methylammonium (CH_3NH_3^+)$, formamidinium (HC $(NH_2)_2^+)$, Cs^+ ; $B^{2+} = Pb^{2+}$, Sn^{2+} ; $X^- = Cl^-$, Br^- , I^-) represent a new class of semiconducting nanomaterials that find applications in solar cell [1], lasers [2], light-emitting diodes [3], and photodetectors [4] due to their stellar set of properties, including tunable emission, high photoluminescence quantum yields (PLQYs), versatile structural control [5]. The ability to precisely tailor the dimension, composition, architecture, and stability, as well as to assemble them into complex yet ordered structures underpin future advances in a wide diversity of optoelectronic materials and devices. To date, much effort has been devoted to the synthesis of perovskite nanocrystals with various sizes, shapes, and compositions, including nanodots [6,7], nanocubes [8], nanorods [9], nanowires [10], and nanoplatelets [11]. As multinary halide salts, perovskite nanocrystals with ionic bonding nature can primarily be synthesized via a high-temperature hot-injection route [12] or a

room-temperature co-precipitation method. In contrast to the former approach that often necessitates an inert atmosphere and a high reaction temperature, the later technique is strikingly facile and thus prevalent. Nevertheless, it still remains challenging to kinetically control and separate the nucleation and growth process of perovskite nanocrystals owing to fast reaction during the co-precipitation process [13,14]. Moreover, the two approaches noted above require a proper surface passivation of perovskite nanocrystals with capping ligands (i.e., oleic acid and oleylamine) to stabilize them for dissolution and dispersion in solutions and thin films. However, due to the highly dynamic binding characteristic, these small molecule ligands can readily dissociate from the surface of perovskite nanocrystals during purification processes especially with the addition of a polar anti-solvent [15]. Consequently, agglomeration and degradation inevitably occur over a long time and thus deteriorate the structural integrity of perovskite nanocrystals upon exposure to moisture, UV irradiation, etc [16].

Among various nanocrystals, hollow nanocrystals possess important advantages over solid counterparts as a result of their large surface to

^{*} Corresponding author.

^{**} Corresponding author.

E-mail addresses: juanpeng@fudan.edu.cn (J. Peng), zhiqun.lin@mse.gatech.edu (Z. Lin).

¹ They contributed equally to this work.

volume ratio, unique geometry with inner negative and outer positive curvatures, high loading capacity, and low density [17]. Several effective strategies capable of synthesizing hollow nanocrystals such as galvanic replacement reactions [18], nanoscale Kirkendall effect [19], Ostwald ripening [20], and sacrificial template-mediated approach have been developed [21]. However, these approaches are limited in scope and applicable primarily to noble-metals, metal oxides, and transition-metal containing sulfides and selenides. In this context, hollow perovskite nanocrystals have not yet been demonstrated. Such hollow nanomaterials may offer new opportunities to interrogate their dimension-dependent optoelectronic properties, and compare with solid counterparts, thereby providing insights into the architecture effect (i.e., solid vs. hollow) on the photophysical properties of this emerging class of nanomaterials. It is notable that the ability to concurrently create uniform solid and hollow perovskite nanocrystals of the same size via a generalizable approach remains a challenging issue.

As noted above, perovskite nanocrystals represent intriguing building blocks for the construction of hierarchical assemblies and materials as well as miniaturized optoelectronic devices [22] via a variety of deposition and patterning techniques (e.g., inkjet printing [23], laser direct writing [24] and lithography [25]). Notably, these widely used techniques possess inherent limitations in arranging nanocrystals over the entire substrate. For example, laser direct writing often involves intricate procedures and expensive equipment for patterning of perovskite nanocrystals, and has low throughput due to its intrinsically serial process nature. More importantly, laser exposure of perovskite nanocrystals inevitably leads to a loss of photoluminescence due to nonradiative recombination as a result of the formation of trap states [26]. While the lithography technique is effective in positioning perovskite nanocrystals, it requires relatively time-consuming, multistep procedures. Moreover, polar solvents (e.g., acetone) that are commonly used in cleaning and lifting off resist can be detrimental to structural integrity of perovskite nanocrystals [25]. Clearly, it is highly desirable to achieve control over the positioning of perovskite nanocrystals with high design complexity (e.g., multicolored consecutive structures) in a simple, inexpensive yet non-invasive manner.

Herein, we developed a robust synthetic strategy for in-situ crafting of stable solid and hollow perovskite quantum dots (PQDs) intimately and permanently ligated with hydrophobic polymers. Specifically, amphiphilic star-like diblock copolymer, poly(acrylic acid)-block-polystyrene (PAA-b-PS) with hydrophilic inner PAA blocks and hydrophobic outer PS blocks and star-like triblock copolymer polystyrene-block-poly (acrylic acid)-block-polystyrene (PS-b-PAA-b-PS) with well-defined molecular weight (MW) of each block and narrow MW distribution are rationally designed and synthesized by sequential atom transfer radical polymerization (ATRP) of the respective monomers. Star-like PAA-b-PS and PS-b-PAA-b-PS are then exploited as unimolecular micellar nanoreactors to preferentially uptake and partition precursors (i.e., lead bromide (PbBr2) and cesium bromide (CsBr) for CsPbBr3) in the compartment occupied by hydrophilic PAA blocks (i.e., a coordination interaction between the metal moieties of precursors and carboxyl groups of PAA), thereby forming a series of stable, monodisperse solid and hollow PQDs of the same external diameter (i.e., tailorable dimension), respectively. As such, it affords a platform to scrutinize the sizeand shape-dependent optical properties of PQDs and implement them in optoelectronic devices (e.g., white LEDs). Notably, the crafted PQDs can be employed as building blocks to yield large-scale regularly arranged stripe-like patterns via a simple meniscus-assisted self-assembly (MASA) approach by constraining the evaporation of the PQDs ink between two nearly parallel plates with the upper blade stationary and the lower substrate movable. Intriguingly, multi-component and emission-tunable stripes can be readily attained via rapid meniscus-assisted anion exchange at selected positions, which may potentially be integrated into fabrication of multifunctional miniaturized optical and optoelectronic devices. Our versatile star-like block copolymer nanoreactor and MASA strategies enable precise control over the dimensions, compositions and

architecture of PQDs and the large-scale construction of periodic patterns of PQDs, respectively, with virtually unlimited material choice, thereby opening up new opportunities to access a myriad of functional nanocrystals and rapidly assemble them for a wide range of applications.

2. Results and discussion

2.1. Structure and morphology analysis

Fig. 1 depicts the two synthetic routes to PS-capped perovskite QDs, that is, all-inorganic solid (route a) and hollow (route b) CsPbBr₃ QDs by capitalizing on amphiphilic unimolecular star-like PAA-b-PS and PS-b-PAA-b-PS, respectively, as nanoreactors (see Experimental Section in Supporting Information). Synthesis of PS-capped hollow CsPbBr3 QDs is selected as an example to elaborate the star-like block copolymer nanoreactor strategy. First, 21-Br-β-CD macroinitiators are prepared by a thorough esterification reaction between hydroxyl groups of β -CD and α-bromoisobutyryl bromide as confirmed by ¹H NMR spectroscopy (Fig. S1). Afterwards, star-like PS-b-PtBA-b-PS triblock copolymer (lower fourth panel; Fig. 1) is synthesized via sequential ATRP of styrene(St), tert-butyl acrylate (tBA), and styrene(St) with controlled MWs and narrow MW distribution of each block emanating from 21-Br-β-CD macroinitiator, as evidenced by monomodal and symmetric gel permeation chromatography (GPC) curves (Fig. S2) (see Experimental Section). The ¹H NMR spectra verified the success in synthesizing star-like PS, PS-b-PtBA, and PS-b-PtBA-b-PS (Figs. S3-S5). The subsequent hydrolysis of intermediate tert-butyl substituents of hydrophobic PtBA blocks yields amphiphilic star-like PS-b-PAA-b-PS triblock copolymer containing hydrophilic PAA blocks. The conversion of star-like PS-b-PtBA-b-PS into PS-b-PAA-b-PS (Fig. S6) was substantiated by ¹H NMR spectroscopy. The MWs of inner PS, intermediate PAA, and outer PS blocks in star-like PSb-PAA-b-PS triblock copolymers and the corresponding dimensions of PS-capped CsPbBr3 QDs are summarized in Table S1. The calculated radius of gyration of star-like polymers and star-like PAA-b-PS polymers matched well with their hydrodynamic diameters from Dynamic light scattering (DLS) (Table S2) which is also the case for star-like PAA-b-PS polymers in the presence of precursors (Table S3), indicating the precursors are accumulated within the unimolecular micelles (Fig. S7). Star-like PS-b-PAA-b-PS is then mixed with CsBr and PbBr₂ in anhydrous DMF at room temperature, during which the metal ions of precursors selectively partition into the hydrophilic PAA compartment via strong coordination interaction with the carboxyl groups of PAA blocks [27], forming CsBr- and PbBr2-loaded star-like PS-b-PAA-b-PS triblock copolymer nanoreactor in DMF (lower second panel; Fig. 1 and Fig. S7). Finally, this DMF solution is dropped into toluene under rigorous stirring to yield PS-capped hollow CsPbBr3 QDs via co-precipitation (i.e., a supersaturation recrystallization process [14,28]; lower first panel in Fig. 1).

Video S1 shows a representative example of the rapid transformation of the precursor-loaded star-like PS-b-PAA-b-PS DMF solution into PScapped hollow CsPbBr₃ QDs in toluene (i.e., poor solvent) solution under UV irradiation at room temperature. Correspondingly, the snapshots shown in Fig. S8 clearly witness such a rapid transition within a few seconds from completely dark to bright green-emitting under UV irradiation. In stark contrast, the CsPbBr3 toluene solution obtained without the introduction of star-like PS-b-PAA-b-PS displays a very weak photoluminescence when the precursor DMF solution is added into toluene. This is due to the formation of large CsPbBr₃ crystals in toluene (see Experimental Section; Fig. S9), substantiating the formation of CsPbBr3 QDs is structure-directed by the intermediate hydrophilic PAA blocks of amphiphilic star-like PS-b-PAA-b-PS triblock copolymer. Similarly, PS-capped solid CsPbBr3 QDs can be synthesized using starlike PAA-b-PS diblock copolymer as nanoreactor (route a; Fig. 1). It is worthy to note that micelles formed by self-assembly of amphiphilic linear block copolymers in selective solvents (i.e., toluene) have been used as nanoreactors for in situ growth of solid PQDs. 28 In comparison,

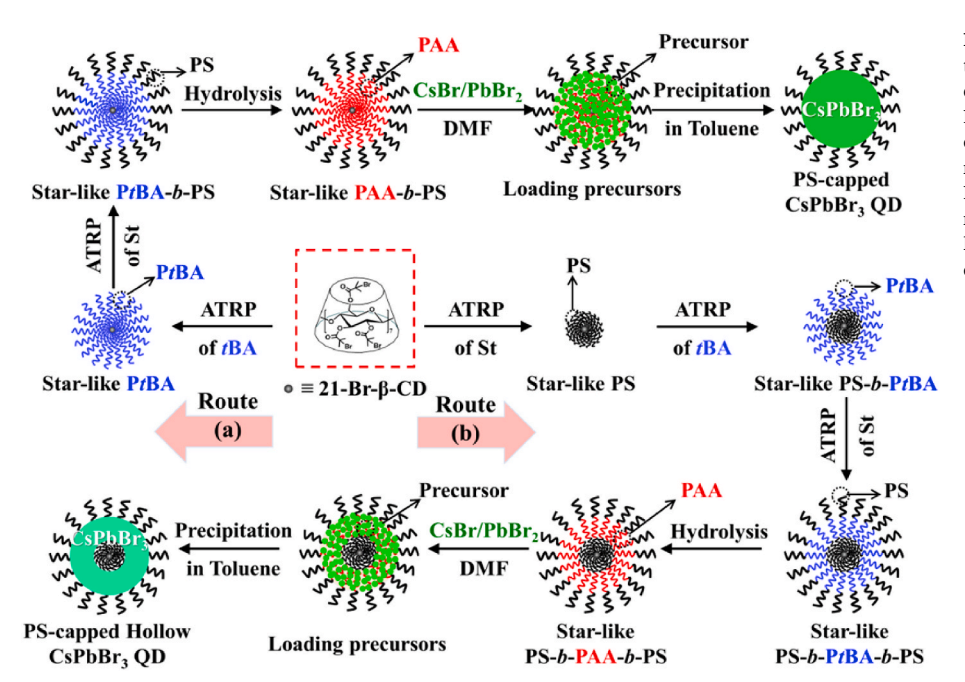


Fig. 1. Stepwise representation of synthetic routes to all-inorganic solid and hollow perovskite quantum dots (PQDs) intimately and permanently ligated with PS chains (i.e., PS-capped solid and hollow PQDs) by capitalizing on amphiphilic star-like copolymers as nanoreactors. Route (a): synthesis of PS-capped solid PQDs using star-like PAA-b-PS diblock copolymer nanoreactor. Route (b): synthesis of PS-capped hollow PQDs with star-like PS-b-PAA-b-PS triblock copolymer nanoreactor.

the amphiphilic linear block copolymers poly(styrene-block-4-vinyl-pyridine) (PS-b-P4VP) also can be applied by two steps process in which linear diblock polymers were first mixed with CsBr and PbBr $_2$ in anhydrous DMF at room temperature to form the precursor solution and then dropped into toluene, forming solid PQDs (Fig. S10). Undoubtedly, only solid QDs can be accessible by usage of amphiphilic linear block copolymers.

Supplementary video related to this article can be found at https://doi.org/10.1016/j.nanoen.2020.105043

Fig. 2a–e shows representative transmission electron microscopy (TEM) images of three PS-capped solid and hollow CsPbBr₃ QDs. By judiciously controlling the ATRP time during the growth of the PtBA blocks (hydrolyzed into PAA later), the dimension of CsPbBr₃ QDs can be readily tailored. For solid CsPbBr₃ QDs (denoted S–CsPbBr₃), they

have an average diameter of 13.6 ± 0.5 nm (Fig. 2a). Two hollow CsPbBr₃ QDs were also crafted, one with an average external diameter of 13.3 ± 0.3 nm and a thick shell thickness of 5.1 ± 0.2 nm (denoted H1–CsPbBr₃; Fig. 2b), and the other with an external diameter of 13.5 ± 0.4 nm and a thin shell thickness of 2.9 ± 0.3 nm (denoted H2–CsPbBr₃; Fig. 2c). Fig. S11 shows the corresponding size distribution histograms of these PS-capped CsPbBr₃ QDs, suggesting monodisperse QDs were obtained. Notably, high-resolution TEM (HRTEM) measurements confirmed the existence of hollow interior in hollow CsPbBr₃ QDs where their center areas appear relatively bright (Fig. S12). The lattice spacing of both solid and hollow CsPbBr₃ QDs is 2.9 Å, which can be indexed to the n(200) plane of the perovskite orthorhombic phase [6], suggesting they are crystalline (Fig. S12 a-c). In contrast, no cavity was seen in zoom-in TEM image and HRTEM for solid CsPbBr₃ QDs (inset in Fig. 2a,

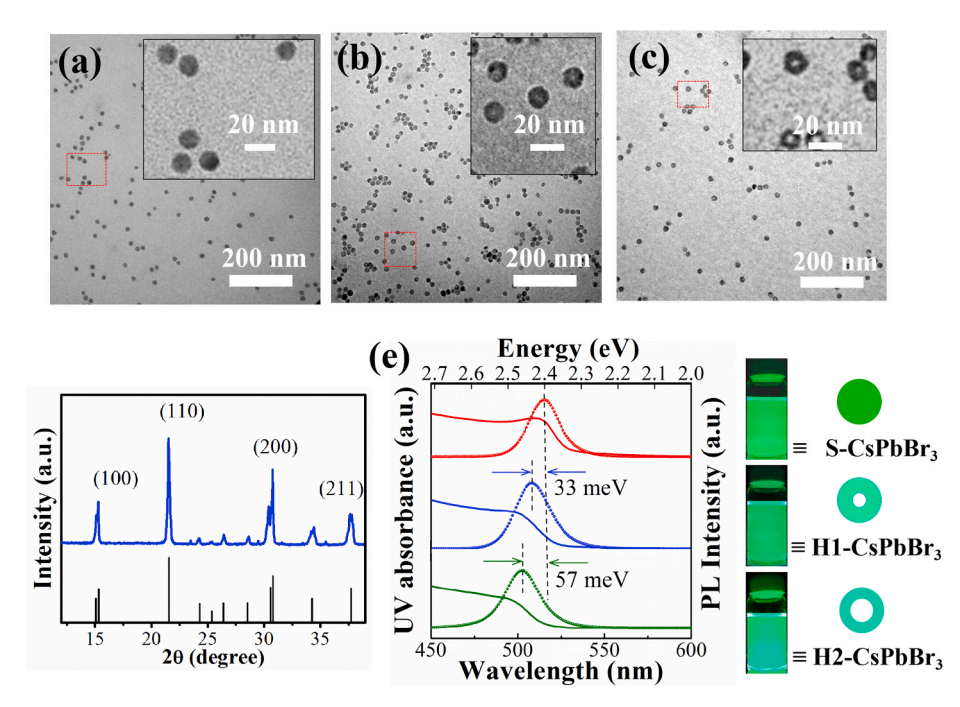


Fig. 2. (a, b, c) TEM images of PS-capped solid and hollow CsPbBr3 QDs crafted by employing amphiphilic star-like block copolymers as nanoreactors. (a) PS-capped solid CsPbBr3 QDs (denoted S-CsPbBr3) with an average external diameter of 13.6 ± 0.5 nm. (b) PS-capped hollow CsPbBr3 QDs with an average external diameter of 13.3 \pm 0.3 nm and shell thickness of 5.1 \pm 0.2 nm (denoted H1–CsPbBr₃). (c) PScapped hollow CsPbBr3 QDs with an external diameter of 13.5 \pm 0.4 nm and shell thickness of 2.9 \pm 0.3 nm (denoted H2-CsPbBr3). (d) Representative Xray diffraction (XRD) pattern of PS-capped H1-CsPbBr3 QDs. (e) UV-vis absorption and PL of PS-capped solid and hollow CsPbBr3 QDs (upper panel: PS-capped S-CsPbBr3; central panel: PScapped H1-CsPbBr3 QDs: lower panel: PS-capped H2-CsPbBr3 QDs). The insets are the respective digital image of each solution under UV light.

Nano Energy 77 (2020) 105043

and Fig. S12a). The presence of hollow interior occupied by the inner PS blocks is due to the fact that these PS chains possess no carboxyl groups to coordinate with the metal ions of perovskite precursors [29]. As hollow QDs differed from nanorings, lattice fringes may also be found in the center area of hollow interior under HRTEM (Fig. S12 b and c). This phenomenon can be attributed to the crystalline shell right above the center hollow interior [17,30]. We also noticed the hollow nanocrystals are polycrystalline rather than forming single crystal due to the retained intermediate PAA chain. For the examination of the PS chains situated on the surface of hollow perovskite surface, the TEM grid was exposed to ruthenium tetraoxide (RuO₄) vapor as stainning agent to preferentially stain the PS chains [31], yielding a grey appearance around hollow QDs (Fig. S13). Representative X-ray diffraction (XRD) profiles of PS-capped CsPbBr3 QDs are shown in Fig. 2d and Fig. S14. These XRD patterns correlate well with the orthorhombic CsPbBr3 QDs synthesized via the co-precipitation method reported in literature [6]. It is noteworthy that hollow CsPbBr3 QDs were formed via a supersaturation crystallization reaction within the star-like triblock copolymer nanoreactors, that is, when a soluble precursor DMF solution is disrupted upon being introduced into anti-solvent toluene solution, the supersaturated ions would rapidly precipitate in the form of nanocrystals [6]. This differs largely from the conventional hot-injection approach utilized to synthesize perovskite CsSnBr₃ nanocages containing a hollow cubic interior with an average size of 100 nm and a shell thickness of 20 nm [32]. The conventional approach not only necessitates high temperature to overcome the higher thermodynamic energy barrier due to the creation of an interior surface but also requires the branched n-alkanoate ligands with strong steric repulsion to increase the solubility of nanocrystals and impart the migration of ions to achieve the limited oriented-attachment for the formation of hollow structures [33]. Clearly, hollow structures created without the use of nanoreactors are comparatively lack of control as its growth invokes a complicated growth-driven self-assembly process [34]. Clearly, our nanoreactor strategy for synthesis of hollow perovskite QDs with tunable thickness is greatly different from the hot-injection method via growth-driven self-assembly.

2.2. Optical properties and WLED devices

As our star-like block copolymer nanoreactor strategy enables the precise engineering of the size of CsPbBr3 QDs as discussed above, we set out to scrutinize the optical properties of as-prepared QDs. Fig. 2e compares the architecture-dependent (i.e., solid vs. hollow) optical properties of three CsPbBr3 QDs. Intriguingly, photoluminescence (PL) peaks of QDs greatly blue-shift as the inner diameter of hollow QDs increases (i.e., decreased shell thickness). The Bohr diameter of CsPbBr3 is ~7 nm [35]. Thus, as the shell thickness decreases (from 7 nm for S–CsPbBr $_3$ to 5.1 \pm 0.2 nm for H1–CsPbBr $_3$, and to 2.9 \pm 0.3 nm for H2-CsPbBr3), the extent of blue-shift was found to be progressively pronounced, representing 33 meV shift for H1-CsPbBr₃ and 57 meV shift for H2-CsPbBr3 compared to S-CsPbBr3 [36]. The absorption onset blue-shifted with decreased thickness of hollow QDs, similar to the blue-shift in the PL spectra. By comparing with a standard Rhodamine 6G sample (QY = 95% in ethanol), the PLQYs of S-CsPbBr₃, H1-CsPbBr₃ and H2-CsPbBr3 were found to be ~71%, 67% and 55%, respectively. Compared to the solid counterpart, the lower PLQY of hollow perovskite QDs could be ascribed to the fact that large surface-to-volume ratio of hollow structures may possess higher density of surface defects. The time-resolved PL (TRPL) decay spectra of solid and hollow CsPbBr₃ QDs are shown in Fig. S15 and Table S4. The decay curves can be fitted bi-exponentially, with average PL lifetimes of obtained QDs comparable to that of nanocubes (average lifetime of \sim 1–22 ns) yet lower than bulk crystal (average lifetime of $\sim\!2500$ ns) [35]. From the PLQY and TRPL measurements, the radiative and nonradiative decay rates of the PS-capped CsPbBr3 solid and hollow QDs were obtained (see Supporting Information, Table S5), respectively. For PS-capped CsPbBr3 solid and hollow QDs, both the nonradiative decay rate and nonradiative decay

rates shows a steady increase as the shell thickness of PQDs decreases, which agrees well with lower PLQY values observed for hollow QDs. These findings are consistent with the static PL measurements, where the blue-shift of PL maxima was observed as the shell thickness of hollow QDs decreases (Fig. 2e). It has been reported that the radiative decay rate increases as the exciton binding energy increases [37]. Thus, the increased radiative decay rate of QDs from S-CsPbBr3, H1-CsPbBr3 to H2-CsPbBr3 suggests the Coulomb interaction between electron and hole pairs (i.e., exciton) is less screened with the decreased shell thickness, and therefore increases the binding energy of QDs [38,39]. Moreover, the increase in the nonradiative decay rate is due to more surface traps at the increased surface area [39]. Clearly, with introduction of inner surface of hollow QDs, the optical properties are less comparable to solid component. However, compared to solid QDs with similar size, hollow QDs represent an interesting class of perovskite nanocrystals with larger surface area and lower material density, imparting structural complexity and enabling the saving of materials and thus cost reduction. In addition, the hollow cavity may act as a light trapper for efficient utilization of the triggering light within white light-emitting diode (WLED).

It is notable that PS-capped CsPbBr₃ QDs crafted using star-like block copolymer nanoreactors also possess high PL quantum yield (PLQY) with narrow full-width-at-half-maximum (~20 nm), rendering them great potential for use in solid-state lighting and displays. The stability of PS-capped CsPbBr3 hollow QDs toluene solution under ambient condition was evaluated prior to the use of these hollow QDs for WLED. The PL intensity of PS-capped H1-CsPbBr3 QDs toluene solution exhibited no obvious intensity change within 3 days and retained 50% of its original value after a one-month storage (Fig. S16). In contrast, oleic acid- and/or oleylamine co-capped CsPbBr3 QDs displayed less than 10% of its original values only after a 24-h storage. The superior stability of PS-capped CsPbBr3 hollow QDs can be attributed to the effective protection by outer hydrophobic and permanently ligated PS chains on the QDs surface. Moreover, the photostability was also assessed by monitoring the PL intensity of PS-capped H1-CsPbBr3 QDs toluene solution under continuous illumination of 450-nm blue light (Fig. S17). As the blue-light exposure time increased, the PL intensity of oleic acidand/or oleylamine co-capped CsPbBr3 QDs decreased significantly and reached 6.2% of its original value at 200 min, which is due primarily to the photo-oxidation and detachment of these small molecule ligands and aggregation of perovskite QDs. In contrast, a 60% retention of its original intensity of PS-capped H1-CsPbBr3 QDs after illumination was obtained, suggesting superior blue-light photostability of PS-capped hollow QDs for WLED application. A representative wide-color gamut prototype WLED was assembled by depositing a layer of a mixture of asprepared green-emitting H1-CsPbBr3 QDs and red-emitting chemical composition-gradient CdSe/Cd_{1-x}Zn_xSe_{1-y}S_y/ZnS QDs [40] and poly (methyl methacrylate) (PMMA) on a blue GaN LED chip as the color converter (see Experimental Section). The CdSe/Cd_{1-x}Zn_xSe_{1-v}S_v/ZnS QDs was chosen as a red-emitting source to prevent possible anion exchange between different perovskite sources. The corresponding PL spectra of the three constituents in the WLED device is shown in Fig. 3a, corresponding to the blue chip (left), H1-CsPbBr3 QDs (center), and CdSe/Cd_{1-x}Zn_xSe_{1-v}S_v/ZnS QDs (right), respectively. A digital image of an actual WLED device emitting white light is shown as an inset (Fig. 3a). Fig. 3b displays the Commission Internationale de L'Eclairage (CIE) diagram of the WLED device. Clearly, a WLED with a CIE coordinate of (0.31, 0.30) and correlated color temperature (CCT) of 7000 K was achieved, close to the standard white color (0.33, 0.33). Notably, the WLED device possesses a much larger color gamut than that of the National Television Systems Committee (NTSC) standard (~1.29 times) (Fig. S18), suggesting a better color quality in terms of hue and saturation may be rendered [8]. Nonetheless, these promising results show great potential of PS-capped CsPbBr3 QDs for fabrication of wide-color gamut display devices.

As-synthesized PS-capped CsPbBr3 QDs can be readily exploited to

S. Pan et al. Nano Energy 77 (2020) 105043

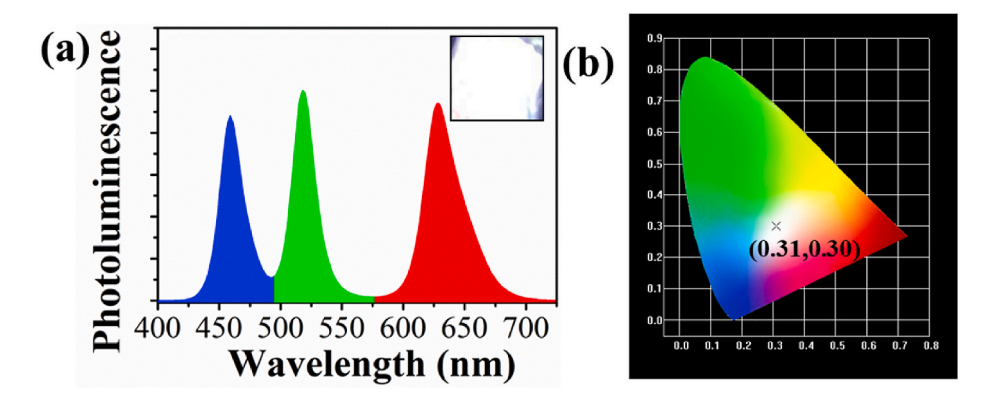


Fig. 3. (a) PL spectra of PS-capped H1–CsPbBr₃ QDs-based white light-emitting diode (WLED) device operated at a current of 10 mA. Inset: the corresponding digital image of WLED, emitting a white light. (b) CIE color diagram of the WLED device.

craft other colloidal CsPbX₃ QDs (X = mixed halide) via convenient anion exchange, affording an additional flexibility to tune the halide compositions and thus the emission color of CsPbX₃ QDs [41]. Taking H1–CsPbBr₃ QDs as the example, their optical properties can be easily altered using ZnCl₂ and ZnI₂ as the Cl⁻ and I⁻ resources to yield hollow blue-emitting CsPb(Cl_xBr_{1-x})₃ and red-emitting CsPb(Br_xI_{1-x})₃, respectively, at low x (Fig. 4a–c). The emission peak λ_{em} of hollow CsPbX₃ progressively shifts from 420 to 675 nm (Fig. 4c) with the smaller λ_{em} corresponding to more Cl content in CsPb(Cl_xBr_{1-x})₃ and the larger λ_{em} for more I content in CsPb(Br_xI_{1-x})₃. Fig. 4b displays the digital images of a set of hollow CsPbX₃ under a 365-nm UV lamp, demonstrating the appealing evolution of emission colors upon forming CsPb(Cl_xBr_{1-x})₃ and CsPb(Br_xI_{1-x})₃ from initial green-emitting H1–CsPbBr₃ QDs.

2.3. Diverse QD patterns via MASA

Due to their outstanding optoelectronic properties, these $CsPbX_3$ QDs (X = Cl, Br, and I or their combinations) represent attractive building blocks for creation of self-assembled nanostructures and patterns with tunable colors for various applications such as solar cells, photodectector, and LEDs [42]. In this context, evaporative self-assembly of nonvolatile solutes (e.g., polymers, DNA, nanoparticles, etc.) from a sessile drop is widely recognized as an extremely simple, nonlithographic route to 1D and 2D structures and assemblies [43]. However, instabilities (e.g., temperature gradient-driven Marangoni flow,

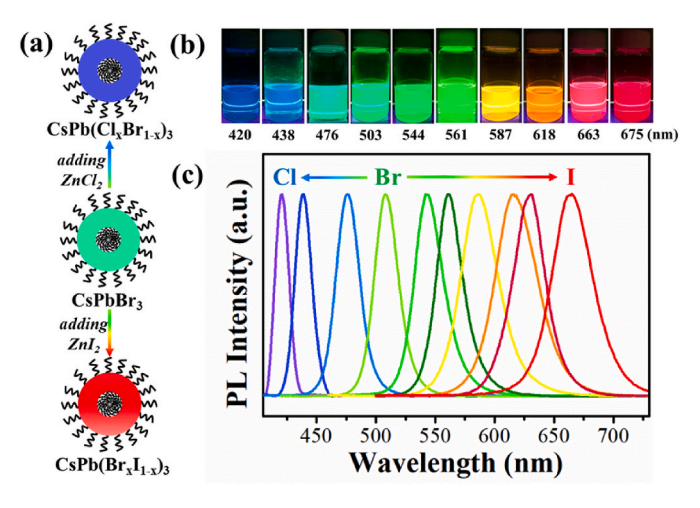


Fig. 4. (a) Schematic illustration of the route from PS-capped H1–CsPbBr $_3$ QDs to PS-capped H1–CsPb(Cl $_x$ Br $_1$ - $_x$) $_3$ QDs and PS-capped H1–CsPb(Br $_x$ I $_1$ - $_x$) $_3$ QDs via anion exchange with ZnCl $_2$ and ZnI $_2$, respectively. (b) Digital images of a series of as-prepared H1-CsPbX $_3$ QDs (X = Br and mixed halides) under UV excitation, and (c) their corresponding photoluminescence (PL) spectra.

fingering instability, etc.) due to unconstrained solvent evaporation on the substrate often result in the formation of randomly assembled structures (e.g., convection cells, fractal branches, and fingerings) [44]. To this end, rather than allowing a droplet to evaporate from a single substrate, a confined geometry composed of two nearly parallel plates in a close proximity with a lower flat Si substrate moving against the upper stationary slightly-tilted plate (i.e., glass blade) in a programmable manner is constructed, where a drop of PS-capped PQD toluene solution is loaded and constrained, forming a capillary-held solution (Fig. 5a). A concave meniscus thus was resulted in (side view in right panel; Fig. 5a) with the separation distance between two plates set at 200 µm. Subjecting the PQD toluene solution to evaporate in such a confined geometry renders the control over solvent evaporation and the associated capillary flow (i.e., a constrained evaporation) and thus a large-scale, meniscus-assisted self-assembly (MASA) of PQDs into regularly ordered patterns with high fidelity.

Taking PS-capped H1-CsPbBr3 QDs as the representative solute example, the repeated "stop-and-move" cycles of lower Si substrate yield periodic stripes of H1-CsPbBr3 QDs. First, the lower Si substrate is kept stationary for a short period of time (i.e., t = 10 s; a "stop" process). During this process, due to the fast evaporative loss of toluene, it creates an evaporative flux with the highest evaporation rate at the edge of meniscus, this triggers an outward convective flow that carries the solutes (i.e., PS-capped H1-CsPbBr3 QDs) to the three-phase contact (i.e., meniscus front), pinning the drying and thus depositing H1-CsPbBr3 QDs to yield a stripe [45]. Subsequently, the lower Si substrate moves laterally (i.e., a "move" process) at a certain speed v (i.e., $v = 100 \, \mu \text{m/s}$) over a distance λ of 50 µm in the direction marked in left panel of Fig. 5a. Meanwhile, the meniscus is stretched, and thus the initial contact angle is reduced to a critical value at which the depinning force is greater than the pinning force [44]. Accordingly, the contact line slips inward to the next new position and resumes the initial contact angle, yielding a new H1-CsPbBr3 QD stripe. Clearly, the repetition of computer-controlled "stop-and-move" cycles effectively produces periodic parallel QD stripes. Specifically, a MASA of 30 μL PS-capped H1-CsPbBr₃ QD toluene solution yields highly ordered QDs stripes over a surface area of 1×1 cm², depending primarily on the size of upper stationary glass blade and the feeding volume of the QD toluene solution. Conceptually, a larger-sized PQD stripe-like pattern can be readily accessed by utilizing a much larger size of upper blade and a continuous feeding of the QD ink into the MASA apparatus. Representative SEM and fluorescence optical micrograph of uniformly distributed PS-capped H1-CsPbBr₃ QD stripes produced by our MASA technique described above are shown in Fig. S19. Clearly, an array of regular stripes over a large area can be readily and rapidly (i.e., less than several minutes) created by one-step MASA, which is remarkably controllable and easy to implement. Fig. S19d shows the line scan of the fluorescence micrograph of H1-CsPbBr3 QD stripes. The fluorescence intensity fluctuates nearly

S. Pan et al. Nano Energy 77 (2020) 105043

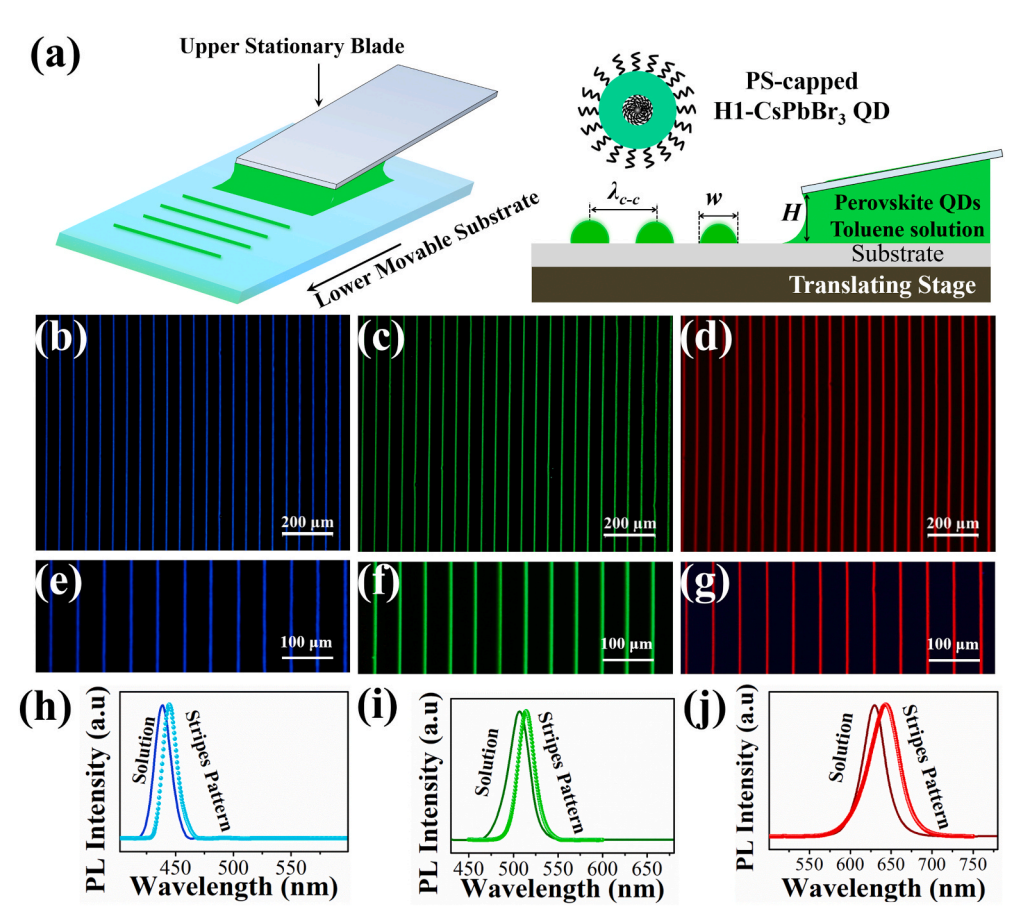


Fig. 5. (a) Schematic illustration of the formation of periodic stripes composed of PScapped H1-CsPbBr3 QDs. Left panel: 3D view. Right panel: side view, where λ_{c-c} is the characteristic distance between the two adjacent stripes formed via meniscusassisted self-assembly (MASA) of a drop of PS-capped H1-CsPbBr3 QDs toluene solution in a two-nearly-parallel-plate geometry in a "stop-and-move" manner. H is the separation distance between the upper glass blade and the lower Si substrate. w is the width of stripes, respectively. (b-j) Representative fluorescence optical micrographs and the corresponding PL spectra of PS-capped hollow $CsPbX_3$ QD (X = Br and mixed halides) stripes over a large area produced by the respective MASA process of PS-capped CsPbX₃ QD toluene solution. (b), (e) and (h) PS-capped H1-CsPb(Cl_xBr_{1-x})₃ QDs. (c), (f) and (i) PS-capped H1-CsPbBr₃ QDs. (d), (g) and (j) PS-capped H1-CsPb(Br_xI_{1-x})₃. The moving speed of the lower Si substrate is 100 um/s, the separation distance between the upper glass blade and the lower Si substrate H is 200 μ m, the stop time is 10 s, and

evenly over a 200 μ m scanning distance, suggesting that the stripes possess uniform height and width. It is worth noting that the distance between two adjacent stripes (λ) can be readily tailored by programing the MASA process with a varied translation distance of lower Si substrate to enable the consecutive "stop-and-move" events. The λ of PS-capped H1–CsPbBr₃ QD stripe of 20, 40, 50, and 100 μ m are shown in Fig. S20a. In addition, as the H1–CsPbBr₃ QD deposition occurs during the stopping time (t_d), the dimension (i.e., width w) of the QD stripes is also dictated by t_d (Fig. S20b).

The ability to rationally construct diverse QD patterns of tunable emissions is of particular interest due to the growing demand for compositional diversity and optical functionality in QD display and other optoelectronic devices [46]. In this context, hollow $CsPbX_3$ (X = Br, Cl_xBr_{1-x} and Br_xI_{1-x}) QD toluene solutions were used as the MASA inks. The stripe patterns with different compositions can be also deliberately formed, emitting blue, green and red fluorescence (Fig. 5b-g). Compared to the respective PL peaks of hollow CsPbX3 QD solutions with a thicker shell (denoted H1-CsPbX $_3$ QDs; X = Br, Cl_xBr_{1-x} and Br_xI_{1-x}), small red-shifts of their films were observed, which can be attributed to the aggregation of QDs during the film deposition (Fig. 5h-j) [47]. Interestingly, the stripes can be easily detached from the Si substrate via ultra-sonication in methanol for several seconds to create the sharp bends and curves in the stripes, which is indicative of their excellent mechanical robustness (Fig. S21). We note that methanol is a poor solvent to promote the surface PS ligands to collapse due to the unfavorable interaction between PS and methanol, thus retaining the stripe-like morphology composed of H1-CsPbBr₃ QDs. Moreover, the dense PS layer situated on surface of perovskite QDs effectively acted as a protective barrier to retard the diffusion of polar organic solvents into CsPbBr₃ QDs, thereby enhancing stability against methanol. In addition, layered stripes with more complex patterns (e.g., diamond, square, etc.)

can also be readily crafted by performing two or three (or even more) MASA processes via rotating the underlying Si substrate to a certain degree for deposition of a second or third set of stripes, respectively (Fig. S22). When small molecular ligand-capped PQDs (e.g., oleic acid-and/or oleylamine-capped PQDs) employed as nonvolatile solute, small molecular ligand-capped PQDs may often yield discontinuous pattern owing to the presence of residual ligands (Fig. S23). Taken together, with introduction of polymer capping, it is expected that other types of polymer-capped QDs with different structures and compositions can also readily form periodic stripes by meniscus-assisted self-assembly.

Due to strong ionic bonding nature of perovskites, both bulk and nanocrystalline forms can inherently undergo a rapid anion exchange at the solid-liquid or solid-vapor interface to yield perovskites with finetuned chemical compositions and optoelectronic properties [48]. In our study, selected-area liquid-solid anion exchange from CsPbBr₃ to CsPb(Cl_xBr_{1-x})₃ or CsPb(Br_xI_{1-x})₃ was achieved by confining the anion exchange reaction with the Cl⁻- or I⁻-containing solution loaded in the two-nearly-parallel-plate geometry, thus spatially directing the formation of multicomponent (i.e., heterojunctioned) hollow CsPbX3 QD stripes, as illustrated in Fig. 6a (see Supporting Information for experimental details). Specially, to create spatially defined heterojunction patterns, stripes of green-emitting H1-CsPbBr₃ QDs are first prepared by the MASA process. Then, a drop of ZnI2 or ZnCl2 toluene solution is loaded and constrained in a two-nearly-parallel-plate geometry with both plates stationary, leading to localized anion exchange on one side of the pre-formed green-emitting stripe pattern. Fig. S24 depicts the mechanism of solid-liquid phase anion exchange. After a short period of selective anion exchange, excess ZnI2 or ZnCl2 toluene solution is removed (Fig. 6a). Fig. 6b-c shows the optical micrographs and the corresponding PL spectra of H1-CsPbBr3 QDs before and after the partial anion exchange with I-, respectively. It is clear that the

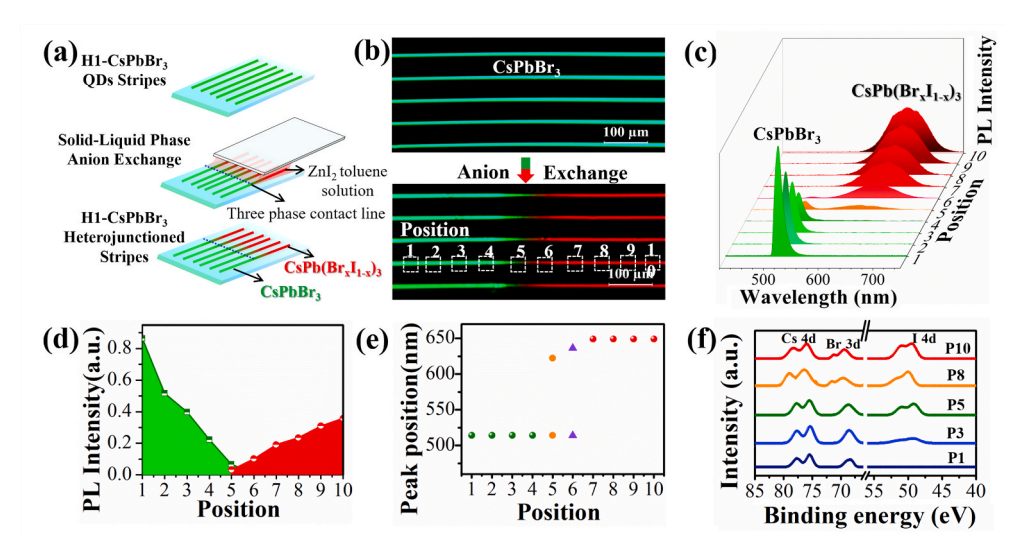


Fig. 6. (a) Schematic illustration of the formation of heterojunctioned H1-CsPbBr₃/ H1-CsPb(Br_xI_{1-x})₃ QD stripes via solid-liquidphase anion exchange. First, the stripes of PS-capped H1-CsPbBr3 QDs are crafted by MASA (upper panel). Then, a drop of ZnI₂ toluene solution is loaded and confined in a two-nearly-parallel-plate geometry with both plates stationary, leading to selective anion exchange localized on one side of the stripe pattern (central panel). After a short period of anion exchange, excess ZnI2 toluene solution is removed to yield heterojunctioned H1-CsPbBr₃/H1-CsPb(Br_xI_{1-x})₃ QD stripes (lower panel). (b) Fluorescence optical micrographs of H1-CsPbBr3 stripes before and after anion exchange. (c) 3D plots of the PL spectra of H1-CsPbBr3 stripes, emitting green (position 1) to red fluorescence (position 10) as a function of the positions marked in (b). (d) The PL intensity and (e) PL peak positions from positions 1 to 10 labeled in (b), respectively. (f) XPS spectra on a heterojunctioned H1-CsPbBr₃/H1-CsPb(Br_xI_{1-x})₃ QD stripes at positions 1, 3, 5, 8, and 10, showing the Cs 4d, Br 3d, and I 4d peaks.

anion-exchanged stripes feature two-color emissions with a gradient interface at the center area. In the Br-to-I exchange sample, the red-emitting stripes has an emission peak centered at 649 nm, corresponding to an approximately 67% Br-to-I conversion. Notably, there is an area (marked as Position 5 and 6 in Fig. 6c and e) possessing two emission peaks assigned to two major peaks of CsPbBr3 and CsPb (Br_xI_{1-x})₃ with varied intensity (Fig. 6d), respectively. To further substantiate the formation of compositionally gradient stripes, the X-ray photoelectron spectroscopy (XPS) measurement was conducted (Fig. 6f). For the CsPbBr3 stripe sample, the peaks of elemental Cs, Pb and Br are clearly seen (bottom curve, Position 1 (P1); Fig. 6f). After anion exchange, the characteristic peaks of I $4d_{3/2}$ and $4d_{5/2}$ at binding energies of 50 eV and 51 eV, respectively, are evident (other curves; Positions 3, 5, 8 and 10 (P3, P5, P8 and P10); Fig. 6f). It is important to note that when performing the XPS scan on the gradient stripes, by focusing on the peaks of Br 3d and I 4d at binding energies of around 69 and 50 eV, respectively, from the P1 to P10, the intensity of the Br 3d peaks was seen to decrease progressively accompanied with the steady increase of the I peaks (Fig. 6f) [49]. The confined anion exchange is simple and effective. It can be readily extended to produce other two-color heterostructures (Fig. S25) by varying the anion source for exchanging (i.e., with Cl ions to create half-green-emitting and half-blue-emitting heterojunctioned stripes, Fig. S25a) and controlling the extent of anion exchange.

3. Conclusion

In summary, we developed a facile amphiphilic star-like block copolymer nanoreactor strategy for *in-situ* crafting of monodisperse polymer-capped solid and hollow PQDs with precisely controlled dimensions, compositions, and architectures. This strategy offers easy access to hollow PQDs that would otherwise be difficult to achieve. Notably, introducing hollow interior to PQDs further extends the ability to tune their optical properties, in addition to the conventional tailoring by the size and the anion exchange of halide compositions of PQDs. Particularly, compared to solid PQDs, the emission of hollow PQDs progressively blue-shifts with increasing diameter of hollow interior. The PQDs of different architectures can be readily implemented for use in LEDs. Furthermore, by judiciously allowing a drop of polymer-capped PQD solution to evaporate in a confined geometry, PQDs can be rapidly and reliably assembled into periodic stripes over large areas via a simple

MASA technique. Intriguingly, multi-colored PQD stripes with gradient heterojunctions can also be conveniently created by constraining the exchange of halide ions of perovskites at selected area. Conceivably, the amphiphilic star-like block copolymer nanoreactor and MASA strategies may offer new opportunities to create a wide variety of uniform polymer-capped functional nanocrystals (e.g., lead-free and organic-inorganic PQDs, semiconducting, plasmonic, magnetic, etc.), as well as to position them into ordered assemblies and patterns. It may be anticipated that the choice of other ligands (e.g., conjugated polymers) may provide opportunities for the resulting polymer-ligated perovskite QDs for use in solar cells or other optoelectronic applications. These nanocrystals and assemblies may find potential applications in photodetectors, sensors, LEDs, solar cells, among other areas.

4. Experimental Section

4.1. Materials

2, 2'-Bipyridyl (bpy, >99%), N,N,N',N",N"-pentamethyldiethylene triamine (PMDETA, 99%), anhydrous 1-methyl-2-pyrrolidinone (NMP, 99.5%), 2-bromoisobutyryl bromide (98%), trifluoroacetic acid (TFA, 99.9%) were purchased from Sigma-Aldrich and used without further purification. Anisole (TCI America, 99.0%), methyl ethyl ketone (MEK, Fisher Scientific, 99.9%), tert-butyl acrylate (tBA, Sigma-Aldrich, 98%) were used without further purification. Styrene (St, Sigma-Aldrich, ≥99%) was purified with 10% NaOH aqueous solution and water consecutively, mixed with anhydrous MgSO4 and CaH2 completely, and distilled under reduced pressure. β-Cyclodextrin (β-CD, Sigma-Aldrich) was dried in a vacuum oven at 80 °C for 12 h before use. Copper(I) bromide (CuBr, Sigma-Aldrich, 98%) was mixed with acetic acid under stirring for 24 h, purified with ethanol and diethyl ether, and then dried under vacuum at room temperature. Poly(styrene)-block-poly(4-vinylpyridine) (PS-b-P4VP; number average molecular weight of PS = 21.0 kg/mol and P4VP = 5.0 kg/mol) was purchased Polymer Source Inc. Lead bromide (PbBr2, 99.9%), cesium bromide (CsBr, 99.999%), oleic acid (OA, 90%), oleylamine (OAm, 70%), anhydrous N, N-dimethylformamide (DMF, 99.8%) were purchased from TCI, STREM Chemicals, Alfa Aesar, Sigma-Aldrich, and Alfa Aesar. Toluene (ACS reagent grade) was obtained from BDH Chemicals. All other reagents were purified by common purification procedures.

4.2. Materials synthesis

4.2.1. Synthesis of 21-arm, star-like poly(acrylic acid)-block-polystyrene (PAA-b-PS) diblock copolymer

4.2.1.1. Synthesis of 21-arm, star-like poly(tert-butyl acrylate) (PtBA) homopolymer. Heptakis[2,3,6-tri-O-(2-bromo-2-methylpropionyl)]16-β-cyclodextrin (i.e., 21Br-β-CD) was synthesized according to our previous works [50]. Typically, CuBr (70.0 mg), PMDETA (170.0 mg), 21Br-β-CD (1000 mg), tBA (42 mL), and MEK (42 mL) were placed in an Ar purged ampule via three freeze-pump-thaw cycles. The ampule was sealed and immersed in an oil bath at 60 °C. After a certain desired time, the reaction was stopped by immersing the ampule in liquid N₂. The mixture was then mixed with THF and passed through a column of neutral alumina to remove the catalyst, and subsequently washed by fractional precipitation with methanol/water (v/v = 1/1) as the precipitator. The product was dried at 40 °C in a vacuum oven for 2 days.

4.2.1.2. Synthesis of 21-arm, star-like poly(tert-butyl acrylate)-block-polystyrene (PtBA-b-PS) diblock copolymer. The reaction mixture at styrene: star-like PtBA (i.e., Br in PtBA macroinitiator): copper bromide: PMDETA = 800: 1: 1: 2 (molar ratio) in anisole (1 g St in 1 mL solvent) was added to an argon purged ampule by three freeze-pump-thaw cycles. The polymerization was performed at 90 °C and stopped by immersing the ampule in liquid N_2 after a certain desired time. The raw product was mixed with THF and passed through a neutral alumina column and washed by fractional precipitation with methanol/water (v/ v = 1/1) as the precipitator. The product was dried at 40 °C under vacuum for 2 days.

4.2.1.3. Synthesis of 21-arm, star-like poly(acrylic acid)-block-polystyrene (PAA-b-PS) diblock copolymer by hydrolysis of star-like PtBA-b-PS [50]. Star-like PtBA-b-PS (0.3 g) was dissolved in 30 mL of CHCl $_3$, followed by the addition of 2.5 mL of trifluoroacetic acid (TFA). After stirring at room temperature for 24 h, the resulting amphiphilic star-like PAA-b-PS diblock copolymer was gradually precipitated in CHCl $_3$. The final product was washed with CHCl $_3$, and thoroughly dried under vacuum at 40 °C.

4.2.2. Synthesis of star-like polystyrene-block-poly(tert-butyl acrylate)-block-polystyrene (PS-b-PAA-b-PS) triblock copolymer

4.2.2.1. Synthesis of 21-arm, star-like polystyrene (PS) homopolymer via the first ATRP. Using as-prepared 21Br- β -CD as the macroinitiator, atom transfer radical polymerization (ATRP) of St monomer (i.e., first ATRP) was conducted for synthesis of star-like PS homopolymer. Briefly, in an ampule purged with argon, CuBr (23.6 mg), bpy (51.3 mg), 21Br- β -CD (32 mg), and St (7 mL) were added. The ampule was degassed via three freeze-pump-thaw cycles in liquid N_2 , sealed, and placed in an oil bath at 90 °C. The reaction was stopped by immersing the ampule in liquid N_2 at different time intervals. The reaction solution was then mixed with THF, passed through a neutral alumina column, and washed via fractional precipitation with THF as solvent and methanol/water (v/v = 1/1) as precipitator. The product was gathered and dried under vacuum at 40 °C for 2 days.

4.2.2.2. Synthesis of 21-arm, star-like polystyrene-block-poly(tert-butyl acrylate) (PS-b-PtBA) diblock copolymer via the second ATRP. Star-like PS-b-PtBA was prepared via ATRP of tBA monomer (i.e., second ATRP) in MEK using star-like PS as the macroinitiator. Typically, the reaction mixture with molar ratio of tBA: star-like PS (i.e., Br group in the macroinitiator): copper bromide: PMDETA = 800:1:1:2 (molar ratio) was dissolved in MEK (1 g tBA in 1 mL solvent) within an ampule filled with Ar and degassed through three freeze-pump-thaw cycles in liquid N₂. Then, the ampule was sealed and immersed in an oil bath at $60\,^{\circ}$ C for

reaction. After a desired polymerization time, the reaction was stopped by immersing the ampule in liquid N_2 . The raw solution was then mixed with THF and passed through a column of neutral alumina, and then washed further by fractional precipitation using THF as solvent and methanol/water (v/v = 1/1) as precipitator. The product was dried under vacuum at 40 $^{\circ}$ C for 2 days.

4.2.2.3. Synthesis of 21-arm, star-like polystyrene-block-poly(tert-butyl acrylate)-block-polystyrene (PS-b-PtBA-b-PS) triblock copolymer via the third ATRP. Star-like PS-b-PtBA-b-PS was prepared via ATRP of St monomer (i.e., third ATRP) in anisole using star-like PS-b-PtBA as the macroinitiator. Briefly, the reaction mixture at St: star-like PS-b-PtBA (i. e., Br group in the macroinitiator): copper bromide: PMDETA = 800:1:1:2 (molar ratio) in anisole (1 g of St in 1 mL of solvent) was added to an ampule protected with Ar via three freeze-pump-thaw cycles in liquid N_2 . Then, the sealed ampule was placed in an oil bath at 90 °C. After a certain desired time, the reaction was stopped by immersing the ampule in liquid N_2 . The crude product was then mixed with THF and passed through a column of neutral alumina and subsequently washed through fractional precipitation by THF as solvent and methanol/water (v/v = 1/1) as precipitator. The yielding product was collected and dried under vacuum at 40 °C for 2 days.

4.2.2.4. Synthesis of amphiphilic 21-arm, star-like polystyrene-block-poly (acrylic acid)-block-polystyrene (PS-b-PAA-b-PS) triblock copolymer via hydrolysis of star-like PS-b-PtBA-b-PS. A typical hydrolysis process was performed as follows: star-like PS-b-PtBA-b-PS (400 mg) was completely dissolved in CHCl $_3$ (40 mL) under stirring at room temperature. Trifluoroacetic acid (TFA, 4 mL) was added dropwise to initiate the hydrolysis. After 24 h, the amphiphilic star-like PS-b-PAA-b-PS triblock copolymer was yielded and gradually precipitated in CHCl $_3$. The collected product was washed with CHCl $_3$, and thoroughly dried in a vacuum oven at 40 °C.

4.2.3. Synthesis of PS-capped solid and hollow perovskite QDs (PQDs) using star-like diblock copolymer and triblock copolymer, respectively, as nanoreactors

A typical synthesis process using star-like copolymer nanoreactor was performed as follows. First, a certain amount of CsBr and PbBr $_2$ was mixed with star-like block copolymer (5 mg/mL) in DMF solution (i.e., precursor DMF solution). The resulting mixture was then incubated at room temperature under gentle stirring (500 rpm) for 24 h at room temperature to upload precursor ions into nanoreactor. Then, a certain amount of the precursor DMF solution (e.g. 50 μ L) was quickly added into toluene (10 mL) under vigorous stirring (800 rpm). Strong green emission of the toluene solution was observed immediately after the injection under UV light. The obatined solution was mildly centrifuged to remove aggregated NCs formed outside nanoreactors.

4.2.4. Synthesis of $CsPbBr_3$ with no ligands via the co-precipitation method at room temperature

CsPbBr $_3$ nanocrystals were synthesized via the co-precipitation method according to the literature with some modifications [14]. In a typical experiment, 0.004 mmol of CsBr, and 0.004 mmol of PbBr $_2$ was added to 10 ml of anhydrous DMF. The solution was ultrasonicated for 1 h or until all precursors dissolved in the solution. Then, the precursor solution was added to toluene to yield CsPbBr $_3$ nanocrystals.

4.2.5. Synthesis of CsPbBr₃ using oleic acid as ligands via the coprecipitation method at room temperature [14]

0.04~mmol of CsBr, and 0.04~mmol of PbBr $_2~\text{mol}$, 1~mL of oleic acid (OA) and 0.5~mL of olylamine (Oam) were dissolved in 10~ml anhydrous DMF. Then, 0.1~mL of the precursor solution was dropped into toluene (1 mL) under stirring. The crude solution was centrifuged at 1000~rpm to remove large particles. The supernatant was subjected to high-speed

centrifugation at 6000 rpm for 10 min with the addition of a small amount of acetone. The precipitate was carefully collected and dispersed in toluene. The centrifugation and dispersion process was repeated for three times.

4.2.6. Synthesis of CsPbBr₃ using P4VP-b-PS via the co-precipitation method at room temperature

A certain amount of CsBr and PbBr $_2$ was mixed with PS-b-P4VP copolymer (5 mg/mL) in DMF solution. The resulting mixture was then stirred at room temperature for 24 h. Then, 50 μ L of the precursor DMF solution was quickly added into toluene (10 mL) under vigorous stirring.

4.2.7. Anion-exchange reaction of PS-capped hollow PQDs

The metal halide solid (ZnCl $_2$ or ZnI $_2$) (10 mg) was dispersed into toluene. We noted that metal-halide salts are hardly solube in toluene. To help metal halide salts to disperse in toluene, fixed amounts of metal halide salts were added into toluene solution under long-time ultrasonication (e.g. 0.5 h) prior to use [51]. With continuous stirring, the respective metal halide solid toluene solution was slowly added into the PS-capped hollow CsPbBr $_3$ QDs (i.e., H1–CsPbBr $_3$ QDs with a thicker shell of 5.1 \pm 0.2 nm) toluene solution. Under UV radiation, a rapid color change can be observed.

4.2.8. Fabrication of WLED devices

Poly(methyl methacrylate) (PMMA), red-emitting $CdSe/Cd_{1-x}Zn_xSe_{1-y}S_y/ZnS$ QDs [40], and green-emitting PS-capped $CsPbBr_3$ H1–CsPbBr $_3$ QDs were mixed using toluene as the solvent. The mixed QDs/PMMA solution was then cast on a GaN blue chip to yield WLED device for further characterizations.

4.2.9. Meniscus-assisted self-assembly of H1-CsPbBr3 QDs toluene solution

A drop of PS-capped H1–CsPbBr $_3$ QDs toluene solution (e.g., 30 µL) was loaded in a two-nearly-parallel-plate geometry constructed by placing an upper glass blade over a lower movable Si substrate with a separation distance of 200 µm. The Si substrate was mounted on a motorized linear translational stage (Parker Hannifin Corp, mode: MX80LVixBL2b). The moving speed (e.g., 100 µm/s) of Si substrate and the stopping time (e.g., 10 s) can be controlled by computer.

4.2.10. Creation of heterojunctioned stripe patterns via selected area liquidsolid anion exchange

To produce stripe patterns with heterojunctions, as-prepared H1–CsPbBr $_3$ QD stripes on Si substrate were placed in the direction orthogonal to the edge of upper glass blade in a two-nearly parallel-plate geometry with a separation distance controlled by a micrometer, of which only a part of stripes are directly under upper glass blade. Then, a drop of ZnI $_2$ or ZnCl $_2$ toluene solution was loaded into the space between the lower Si substrate and the upper glass blade, from which anion exchange of Br $^-$ with either Cl $^-$ or I $^-$ occurred. After a few seconds, excess ZnI $_2$ or ZnCl $_2$ toluene solution was removed.

4.3. Characterizations

The number average molecular weight, $M_{\rm ID}$, and polydispersity index, PDI, of as-prepared star-like polymers were measured by gel permeation chromatography (GPC) equipped with a LC-20AD HPLC pump and a refractive index detector (RID-10A, 120V) at 35 °C. A series of standard samples, monodisperse polystyrene, were used to calibrate GPC. The flow rate of eluent THF was set at 1.0 mL/min⁻¹. Proton nuclear magnetic resonance (1 H NMR) spectra were recorded on a Varian VXR-300 spectroscope using CDCl₃ or d₇-DMF as solvent.

The size distribution and morphology of PS-capped solid and hollow PQDs were obtained by transmission electron microscope (TEM) (JEOL 100; operated at 100 kV) and high-resolution transmission electron microscope (HRTEM, TECNAIG 2 F30; operated at 200 kV). TEM samples were made by dropping solution containing PQDs onto a carbon-coated

copper TEM grid (300 mesh) and dried at room temperature. The optical properties of PQDs were determined by UV-vis spectroscopy (Varian; UV-vis-NIR spectrophotometer, Cary 5000) and PL (Shimadzu fluorescent RF-5301PC spectrofluorophotometer). The crystalline structures of PQDs were evaluated by X ray diffraction (XRD, X'pert PRO, Netherlands). Lifetime measurements (Time-resolved luminescence) were performed using a Photon Technology International Laserstrobe Spectrofluorometer (PTI GL-3300 ns nitrogen laser $\lambda = 337$ nm; photomultiplier tube; time-correlated single photon counting). For TRPL test, each sample was run at the same irradiation intensity for 30 s to collect data. The deduction of background was conducted for each sample. WLED measurements were conducted using a spectral irradiance meter (SIM-2 Plus). UV lamp at 365 nm (4W, UVGL-25) was used to excite PQDs. Optical image and fluorescence optical micrograph of uniformly distributed PQD stripes were obtained by optical microscope (Olympus BX51). The photoluminescence spectra of PQD patterns were determined from hyperspectral datacubes, which were collected using a CytoViva Hyperspectral scanning system using a diffraction grating spectrophotometer (spectral range of 400–1000 nm). The evolution of the PL intensity and wavelength of the CsPbX3 stripes pattern was examined under a continuous light exposure. X ray photoelectron spectroscopy (XPS) measurements were performed on a Thermo K-alpha electron spectrometer with Al Ka radiation. Colloidal stability was studied by measuring the PL intensity after storing the PS-capped H1-CsPbBr3 QDs and OA- and OAm-cocapped CsPbBr3 QDs toluene for different times under ambient condition. The solutions were kept still and exposed to air. Photostability was tested by measuring the PL intensity after continuous illumination with 450 nm blue-light (12 W).

The authors declare no competing financial interest.

Declaration of competing interest

The authors declare that they have no known competing financial interests or personal relationships that could have appeared to influence the work reported in this paper.

CRediT authorship contribution statement

Shuang Pan: Writing - original draft. Yihuang Chen: Writing - original draft. Zewei Wang: Formal analysis. Yeu-Wei Harn: Formal analysis. Jiwoo Yu: Formal analysis. Aurelia Wang: Formal analysis. Marcus J. Smith: Formal analysis. Zili Li: Formal analysis. Vladimir V. Tsukruk: Formal analysis. Juan Peng: Writing - review & editing. Zhiqun Lin: Writing - review & editing.

Acknowledgements

This work is supported by by the AFOSR (FA9550-19-1-0317), the NSF (CMMI 1727313 and 1914713, CBET 1803495, and ECCS 1914562) and the National Natural Science Foundation of China (Grant No: 21922503). S.P. and Y.C. contributed equally to this work.

Appendix A. Supplementary data

Supplementary data to this article can be found online at https://doi.org/10.1016/j.nanoen.2020.105043.

References

- Q. Zhao, A. Hazarika, X. Chen, S.P. Harvey, B.W. Larson, G.R. Teeter, J. Liu, T. Song, C. Xiao, L. Shaw, Nat. Commun. 10 (1) (2019) 2842, https://doi.org/ 10.1038/s41467-019-10856-z.
- [2] P. Liu, X. He, J. Ren, Q. Liao, J. Yao, H. Fu, ACS Nano 11 (6) (2017) 5766–5773, https://doi.org/10.1021/acsnano.7b01351.
- [3] Y.H. Kim, H. Cho, T.W. Lee, Proc. Natl. Acad. Sci. U.S.A. 113 (42) (2016) 11694–11702, https://doi.org/10.1073/pnas.1607471113.
- [4] H. Wang, D.H. Kim, Chem. Soc. Rev. 46 (17) (2017) 5204–5236, https://doi.org/ 10.1039/c6cs00896h.

- [5] Q.A. Akkerman, G. Raino, M.V. Kovalenko, L. Manna, Nat. Mater. 17 (5) (2018) 394–405, https://doi.org/10.1038/s41563-018-0018-4.
- [6] S. Sun, D. Yuan, Y. Xu, A. Wang, Z. Deng, ACS Nano 10 (3) (2016) 3648–3657, https://doi.org/10.1021/acsnano.5b08193.
- [7] Y. He, Y.J. Yoon, Y.W. Harn, G.V. Biesold-McGee, S. Liang, C.H. Lin, V.V. Tsukruk, N. Thadhani, Z. Kang, Z. Lin, Sci. Adv. 5 (11) (2019), eaax4424, https://doi.org/ 10.1126/sciady.aax4424
- [8] L. Protesescu, S. Yakunin, M.I. Bodnarchuk, F. Krieg, R. Caputo, C.H. Hendon, R. X. Yang, A. Walsh, M.V. Kovalenko, Nano Lett. 15 (6) (2015) 3692–3696, https://doi.org/10.1021/nl5048779.
- [9] S. Aharon, L. Etgar, Nano Lett. 16 (5) (2016) 3230–3235, https://doi.org/10.1021/acs.nanolett.6b00665.
- [10] D. Zhang, Y. Yu, Y. Bekenstein, A.B. Wong, A.P. Alivisatos, P. Yang, J. Am. Chem. Soc. 138 (40) (2016) 13155–13158, https://doi.org/10.1021/jacs.6b08373.
- [11] S. Yang, W. Niu, A.L. Wang, Z. Fan, B. Chen, C. Tan, Q. Lu, H. Zhang, Angew. Chem. Int. Ed. 56 (15) (2017) 4252–4255, https://doi.org/10.1002/ anje.201701134.
- [12] Y. Bekenstein, B.A. Koscher, S.W. Eaton, P. Yang, A.P. Alivisatos, J. Am. Chem. Soc. 137 (51) (2015) 16008–16011, https://doi.org/10.1021/jacs.5b11199.
- [13] F. Zhang, C. Chen, S.V. Kershaw, C. Xiao, J. Han, B. Zou, X. Wu, S. Chang, Y. Dong, A.L. Rogach, H. Zhong, ChemNanoMat 3 (5) (2017) 303–310, https://doi.org/ 10.1002/cnma.201700034.
- [14] X. Li, Y. Wu, S. Zhang, B. Cai, Y. Gu, J. Song, H. Zeng, Adv. Funct. Mater. 26 (15) (2016) 2435–2445, https://doi.org/10.1002/adfm.201600109.
- [15] J. De Roo, M. Ibáñez, P. Geiregat, G. Nedelcu, W. Walravens, J. Maes, J.C. Martins, I. Van Driessche, M.V. Kovalenko, Z. Hens, ACS Nano 10 (2) (2016) 2071–2081, https://doi.org/10.1021/acsnano.5b06295.
- [16] S. Huang, Z. Li, B. Wang, N. Zhu, C. Zhang, L. Kong, Q. Zhang, A. Shan, L. Li, ACS Appl. Mater. Interfaces 9 (8) (2017) 7249–7258, https://doi.org/10.1021/ acsami.6b14423.
- [17] Y. Chen, D. Yang, Y.J. Yoon, X. Pang, Z. Wang, J. Jung, Y. He, Y.W. Harn, M. He, S. Zhang, G. Zhang, Z. Lin, J. Am. Chem. Soc. 139 (37) (2017) 12956–12967, https://doi.org/10.1021/jacs.7b04545.
- [18] Y. Sun, Y. Xia, J. Am. Chem. Soc. 126 (12) (2004) 3892–3901, https://doi.org/ 10.1021/ja039734c.
- [19] Y. Yin, R.M. Rioux, C.K. Erdonmez, S. Hughes, G.A. Somorjai, A.P. Alivisatos, Science 304 (5671) (2004) 711–714, https://doi.org/10.1126/science.1096566.
- [20] H.C. Zeng, J. Mater. Chem. 16 (7) (2006) 649–662, https://doi.org/10.1039/ R511296F
- [21] E. Prodan, C. Radloff, N.J. Halas, P. Nordlander, Science 302 (5644) (2003) 419-422. https://doi.org/10.1126/science.1089171.
- 419-422, https://doi.org/10.1126/science.1089171.
 [22] M.V. Kovalenko, L. Protesescu, M.I. Bodnarchuk, Science 358 (6364) (2017) 745-750. https://doi.org/10.1126/science.aam7093.
- [23] B.H. Kim, M.S. Onses, J.B. Lim, S. Nam, N. Oh, H. Kim, K.J. Yu, J.W. Lee, J.H. Kim, S.K. Kang, C.H. Lee, J. Lee, J.H. Shin, N.H. Kim, C. Leal, M. Shim, J.A. Rogers, Nano Lett. 15 (2) (2015) 969–973, https://doi.org/10.1021/nl503779e.
- [24] F. Palazon, Q.A. Akkerman, M. Prato, L. Manna, ACS Nano 10 (1) (2016) 1224–1230, https://doi.org/10.1021/acsnano.5b06536.
- [25] C.H. Lin, Q. Zeng, E. Lafalce, S. Yu, M.J. Smith, Y.J. Yoon, Y. Chang, Y. Jiang, Z. Lin, Z.V. Vardeny, Adv. Opt. Mater. 6 (16) (2018), 1800474, https://doi.org/ 10.1002/adom.201800474.
- [26] J. Chen, Y. Wu, X. Li, F. Cao, Y. Gu, K. Liu, X. Liu, Y. Dong, J. Ji, H. Zeng, Adv. Mater. Techno. 2 (10) (2017), 1700132, https://doi.org/10.1002/admt.201700132.
- [27] Y. Chen, Z. Wang, Y. He, Y.J. Yoon, J. Jung, G. Zhang, Z. Lin, Proc. Natl. Acad. Sci. U.S.A. 115 (7) (2018) E1391–E1400, https://doi.org/10.1073/pnas.1714748115.
- [28] Y. Liu, Z. Wang, S. Liang, Z. Li, M. Zhang, H. Li, Z. Lin, Nano Lett. 19 (12) (2019) 9019–9028, https://doi.org/10.1021/acs.nanolett.9b04047.
- [29] X. Pang, L. Zhao, W. Han, X. Xin, Z. Lin, Nat. Nanotechnol. 8 (6) (2013) 426, https://doi.org/10.1038/nnano.2013.85.
- [30] S. Peng, S. Sun, Angew. Chem. Int. Ed. 46 (22) (2007) 4155–4158, https://doi.org/ 10.1002/anie.200700677.
- [31] J.S. Trent, J.I. Scheinbeim, P.R. Couchman, Macromolecules 16 (4) (1983) 589–598, https://doi.org/10.1021/ma00238a021.
- [32] A. Wang, Y. Guo, F. Muhammad, Z. Deng, Chem. Mater. 29 (15) (2017) 6493–6501, https://doi.org/10.1021/acs.chemmater.7b02089.
- [33] G. Jia, A. Sitt, G.B. Hitin, I. Hadar, Y. Bekenstein, Y. Amit, I. Popov, U. Banin, Nat. Mater. 13 (3) (2014) 301, https://doi.org/10.1038/nmat3867.
- [34] T. Udayabhaskararao, M. Kazes, L. Houben, H. Lin, D. Oron, Chem. Mater. 29 (3) (2017) 1302–1308, https://doi.org/10.1021/acs.chemmater.6b04841.
- [35] F. Zhang, H. Zhong, C. Chen, X.-g. Wu, X. Hu, H. Huang, J. Han, B. Zou, Y. Dong, ACS Nano 9 (4) (2015) 4533–4542, https://doi.org/10.1021/acsnano.5b01154.
- [36] Y. Dong, T. Qiao, D. Kim, D. Parobek, D. Rossi, D.H. Son, Nano Lett. 18 (6) (2018) 3716–3722, https://doi.org/10.1021/acs.nanolett.8b00861.
- [37] J. Feldmann, G. Peter, E. Göbel, P. Dawson, K. Moore, C. Foxon, R. Elliott, Phys. Rev. Lett. 59 (20) (1987) 2337, https://doi.org/10.1103/PhysRevLett.59.2337.
- [38] G. Bastard, E. Mendez, L. Chang, L. Esaki, Phys. Rev. B 26 (4) (1982), https://doi. org/10.1103/PhysRevB.26.2247, 1974.
- [39] Y. Tong, F. Ehrat, W. Vanderlinden, C. Cardenas-Daw, J.K. Stolarczyk, L. Polavarapu, A.S. Urban, ACS Nano 10 (12) (2016) 10936–10944, https://doi. org/10.1021/acsnano.6b05649.
- [40] J. Jung, C.H. Lin, Y.J. Yoon, S.T. Malak, Y. Zhai, E.L. Thomas, V. Vardeny, V. V. Tsukruk, Z. Lin, Angew. Chem. Int. Ed. 55 (16) (2016) 5071–5075, https://doi.org/10.1002/anie.201601198.

- [41] G. Nedelcu, L. Protesescu, S. Yakunin, M.I. Bodnarchuk, M.J. Grotevent, M. V. Kovalenko, Nano Lett. 15 (8) (2015) 5635–5640, https://doi.org/10.1021/acs.nanolett.5b02404.
- [42] D.Y. Lee, J.T. Pham, J. Lawrence, C.H. Lee, C. Parkos, T. Emrick, A.J. Crosby, Adv. Mater. 25 (9) (2013) 1248–1253, https://doi.org/10.1002/adma.201203719.
- [43] B. Li, W. Han, B. Jiang, Z. Lin, ACS Nano 8 (3) (2014) 2936–2942, https://doi.org/ 10.1021/nn500193v.
- [44] W. Han, M. Byun, B. Li, X. Pang, Z. Lin, Angew. Chem. Int. Ed. 51 (50) (2012) 12588–12592, https://doi.org/10.1002/anie.201207902.
- [45] J. Xu, J. Xia, S.W. Hong, Z. Lin, F. Qiu, Y. Yang, Phys. Rev. Lett. 96 (6) (2006), 066104
- [46] T.-H. Kim, K.-S. Cho, E.K. Lee, S.J. Lee, J. Chae, J.W. Kim, D.H. Kim, J.-Y. Kwon, G. Amaratunga, S.Y. Lee, B.L. Choi, Y. Kuk, J.M. Kim, K. Kim, Nat. Photon. 5 (3) (2011) 176–182, https://doi.org/10.1038/nphoton.2011.12.
- [47] F. Di Stasio, M. Imran, Q.A. Akkerman, M. Prato, L. Manna, R. Krahne, J. Phys. Chem. Lett. 8 (12) (2017) 2725–2729, https://doi.org/10.1021/acs. ipclett.7b01305.
- [48] L. Dou, M. Lai, C.S. Kley, Y. Yang, C.G. Bischak, D. Zhang, S.W. Eaton, N. S. Ginsberg, P. Yang, Proc. Natl. Acad. Sci. U.S.A 114 (28) (2017) 7216–7221, https://doi.org/10.1073/pnas.1703860114.
- [49] A. Haque, V.K. Ravi, G.S. Shanker, I. Sarkar, A. Nag, P.K. Santra, J. Phys. Chem. C 122 (25) (2017) 13399–13406, https://doi.org/10.1021/acs.jpcc.7b11118.
- [50] X. Pang, L. Zhao, M. Akinc, J.K. Kim, Z. Lin, Macromolecules 44 (10) (2011) 3746–3752, https://doi.org/10.1073/pnas.1703860114.
- [51] T. Zhang, G. Li, Y. Chang, X. Wang, B. Zhang, H. Mou, Y. Jiang, CrystEngComm 19 (8) (2017) 1165–1171, https://doi.org/10.1039/C6CE02314B.



Shuang Pan received his B.S (2013) in Materials Science and Engineering from Shandong University of technology and Ph.D. (2018) in Macromolecular Science from Fudan University. Dr. Shuang Pan is a currently postdoctoral fellow in the Department of Macromolecular Science at Fudan University. She has been a visiting researcher in Prof. Zhiqun Lin's group at the Georgia Institute of Technology from 2016 to 2019. Her current research focuses on synthesis, self-assembly, and patterning of perovskite materials for use in LEDs and photodetectors.



Yihuang Chen received his B.E. (2013) and PhD (2017) in Materials Science and Engineering with Prof. Guangzhao Zhang from South China University of Technology. From 2017 to 2019 he was a Postdoctoral Fellow in Prof. Zhiqun Lin's group at the Georgia Institute of Technology. His research interests mainly focus on the synthesis of responsive bulk polymers, functional polymer brushes, and polymer/inorganic nanocrystal hybrids for applications in controlled drug release and catalysis.



Zewei Wang received his B.S (2013) in Applied Chemistry from Shanghai Jiao Tong University, M.S (2014) in Polymer Science from the University of Akron, and Ph.D. (2019) in Materials Science and Engineering with Prof. Zhiqun Lin from Georgia Institute of Technology. He is now (2019) working as a packaging engineer at Intel, USA. His research interests mainly focus on design and synthesis of architectured block copolymers and nanocrystals for energy storage and electrocatalysis.

S. Pan et al. Nano Energy 77 (2020) 105043



Yeu-Wei Harn received her bachelor's degree in a double specialty program of Management and Technology with double specialties in materials science and engineering and quantitative finance in 2013 and her master's degree in materials science and engineering in 2015, both from National Tsing Hua University in Taiwan. After that, she entered Georgia Institute of Technology and is currently working as a Ph.D. candidate of materials science and engineering under Professor Zhiqun Lin. Her work focuses on using soft star-like diblock and/or triblock copolymers as nanoreactors to synthesize functional nanoparticles and the subsequent investigation of their ferroelectric, magnetic and electrocatalytic properties.



Vladimir V. Tsukruk is a Regents Professor and Dean's Professor of Engineering, and Director of Microanalysis Center at the School of Materials Science and Engineering, Georgia Institute of Technology, Atlanta, USA. He received MS degree in physics from the National University of Ukraine, PhD and DSc degrees in polymer science from the National Academy of Sciences of Ukraine. He carried out his post-doctoral research at the U. Marburg, Darmstadt TU and U. Akron. His research focuses on in the field of hybrid nanomaterials, surfaces and interfaces, directed assembly of synthetic/natural polymers and nano-structures, biomimetic designs, and bioinspired nanomaterials.



Jiwoo Yu received her B.S. degree at the University of Illinois at Urbana-Champaign in 2014 and M.S. degree at Seoul National University in 2016 in Materials Science and Engineering. She is currently a Ph.D. candidate in Materials Science and Engineering at the Georgia Institute of Technology under the advisement of Dr. Zhiqun Lin. Her research interest includes nanomaterials, polymers, renewable materials, self-assembly, and nanopatterning.



Juan Peng is a Professor in the Department of Macromolecular Science at Fudan University. She received her PhD in State Key Laboratory of Polymer Physics and Chemistry from Changchun Institute of Applied Chemistry, Chinese Academy of Sciences in 2005. Her research interests include conjugated polymers, block copolymers, polymer-based nanocomposites, hierarchical structures, and functional nanocrystals.



Aurelia Wang received her B.S. in Biochemistry from the Georgia Institute of Technology. After working in medical genetics, she returned to the Georgia Institute of Technology to work on her PhD in materials science and engineering under the supervision of Prof. Zhiqun Lin and Prof. Zhong Lin Wang. Her research interests include energy harvesting with nanogenerators and self-powered smart devices. Her research focuses on the materials aspect of triboelectric nanogenerators and the mechanism of contact electrification.



Zhiqun Lin is a Professor in the School of Materials Science and Engineering at the Georgia Institute of Technology. He received his Ph.D. degree in Polymer Science and Engineering from the University of Massachusetts, Amherst in 2002. His research interests include electrocatalysis, photocatalysis, solar cells, lithium ion batteries, semiconductor organic-inorganic nanocomposites, quantum dots (rods), multifunctional nanocrystals, Janus nanostructures, conjugated polymers, block copolymers, polymer blends, hierarchical structure formation and assembly, and surface and interfacial properties.



Zili Li was born in Anhui, China. He received his BS degree in Materials Science and Engineering from Zhengzhou University and Ph.D. degree in Chemistry from University of Science and Technology of China in 2017. Now he is doing postdoctoral research in the School of Materials Science and Engineering at the Georgia Institute of Technology. His research focuses on the synthesis of self-healing soft matters, 2D polymers, and nanocrystals for electrocatalysis and plasmonics.